European Journal of Pharmaceutics and Biopharmaceutics 204 (2024) 114512

Contents lists available at ScienceDirect

European Journal of Pharmaceutics and Biopharmaceutics

journal homepage: www.elsevier.com/locate/ejpb

Inhalable nano-structured microparticles for extracellular matrix modulation as a potential delivery system for lung cancer

Salma M. Abdel-Hafez [a,b], Markus Gallei [c,d], Sylvia Wagner [e], Marc Schneider [a,*]

[a] Department of Pharmacy, Biopharmaceutics and Pharmaceutical Technology, Saarland University, 66123 Saarbrücken, Germany
[b] Department of Pharmaceutics and Industrial Pharmacy, Faculty of Pharmacy, Ain Shams University, 11566 Cairo, Egypt
[c] Polymer Chemistry, Saarland University, 66123 Saarbrücken, Germany
[d] Saarene, Saarland Center for Energy Materials and Sustainability, 66123 Saarbrücken, Germany
[e] Department Bioprocessing and Bioanalytics, Fraunhofer Institute for Biomedical Engineering IBMT, 66280 Sulzbach, Germany

ARTICLE INFO

Keywords:
Nano-embedded microparticles
Nano-in-microparticles
Trojan particles
Spray drying
Nanoparticle penetration
Adenocarcinoma spheroid model
Lung cancer therapy

ABSTRACT

The use of inhalable nanoparticulate-based systems in the treatment of lung cancer allows for efficient localized delivery to the lungs with less undesirable systemic exposure. For this to be attained, the inhaled particles should have optimum properties for deposition and at the same time avoid pulmonary clearance mechanisms. Drug delivery to solid tumors is furthermore challenging, due to dense extracellular matrix (ECM) formation, which hinders the penetration and diffusion of therapeutic agents. To this end, the aim of the current work is to develop an ECM-modulating nano-structured microparticulate carrier, that not only enables the delivery of therapeutic nanoparticles (NPs) to the lungs, but also enhances their intratumoral penetration. The system is composed of acetalated maltodextrin (AcMD) NPs embedded into a water-soluble trehalose/leucine matrix, in which collagenase was loaded with different mass concentrations (10 %, 30 % and 50 %). The collagenase-containing AcMD nano-structured microparticles (MPs) exhibited suitable median volume diameters (2.58 ± 1.35 to 3.01 ± 0.68 μm), hollow corrugated morphology, sufficient redispersibility, low residual moisture content (2.71 ± 0.17 % to 3.10 ± 0.20 %), and favorable aerodynamic properties (Mass median aerodynamic diameter (MMAD): 1.93 ± 0.06 to 2.80 ± 0.10 μm and fine particle fraction (FPF): 68.02 ± 6.86 % to 69.62 ± 2.01 %). Importantly, collagenase retained as high as 89.5 ± 6.7 % of its enzymatic activity after spray drying. MPs containing 10 % mass content of collagenase did not show signs of cytotoxicity on either human lung adenocarcinoma A549 cells or lung MRC-5 fibroblasts. The nanoparticle penetration was tested using adenocarcinoma A549/MRC-5 co-culture spheroid model, where the inclusion of collagenase resulted in deeper penetration depth of AcMD-NPs.

1. Introduction

Lung cancer is the second most diagnosed cancer worldwide, representing 11.4 % of all malignancies. In terms of mortality, lung cancer is the leading cause of cancer-related deaths with 18.0 % mortality [1,2]. Lung cancer is classically categorized into two histological types: small cell lung cancer (SCLC) and non-small cell lung cancer (NSCLC), accounting for approximately 15 % and 85 % of all lung cancer incidences, respectively [3,4]. The more frequent NSCLC is mainly subclassified into adenocarcinoma, squamous cell carcinoma, and large cell carcinoma (40 %, 25 – 30 % and 10 – 15 % of the total lung cancer cases, respectively) [5,6]. In addition to the cytopathological aspects, lung cancer subtypes differ with respect to the location at which they develop in the lungs. While most SCLC and squamous cell carcinoma tumors tend to locate centrally [7,8], adenocarcinomas develop in the bronchiolar and alveolar regions and hence are mainly more peripherally located [8,9]. Therapeutic alternatives for lung cancer include surgical resection, radiotherapy, chemotherapy, and to date, targeted therapy and immunotherapy. Whether applied alone or in combination with other interventions, intravenous chemotherapy is a main part of the treatment regimen in most lung cancer cases [10,11]. However, poor therapeutic response is usually observed due to suboptimal drug concentrations in the cancerous lung tissue, coupled with the occurrence of systemic side effects that cause treatment interruptions and thereby repeated proliferation and invasion of malignant cells [12]. Through achieving higher drug concentrations in the lungs and limiting systemic exposure, the

* Corresponding author at: Saarland University Campus C4 1, 66123 Saarbrücken, Germany.
E-mail address: Marc.Schneider@uni-saarland.de (M. Schneider).

https://doi.org/10.1016/j.ejpb.2024.114512
Received 30 November 2023; Received in revised form 13 September 2024; Accepted 20 September 2024
Available online 26 September 2024

pulmonary route provides a dual solution to the drawbacks of systemic administration [13]. Additionally, the pulmonary route avoids first pass metabolism and is characterized by better patient compliance, as it is needle-free and may not require hospitalization [14].

Utilization of nanocarriers for pulmonary delivery of chemotherapeutics could circumvent several drawbacks of conventional inhalation chemotherapy (for example, in the form of solution or suspension). Nanocarriers could control the release of the loaded anticancer drugs, thus avoiding abrupt high concentrations that induce lung toxicity. Moreover, they enable targeted and specific bioresponsive delivery by tailoring their design, composition, and physicochemical properties, which would potentially avoid or decrease non-specific interaction with healthy lung tissues [14–16]. Nebulization is a straightforward approach to deliver nanocarriers, however it has its shortcomings regarding the restricted portability, the lengthy time of administration, and the formulation being in the liquid state, which may pose stability and contamination issues [17,18]. Pressurized metered-dose inhalers (pMDI) and soft mist inhalers (SMI) are not easily adaptable for lung cancer treatment, due to their limited capability to deliver drug doses in the microgram range [12]. The use of dry powder inhalers (DPI) provides several benefits compared to the prementioned inhalers. Besides the better long-term physical stability of the formulation and the loaded drug, DPIs can deliver high drug doses, actuated by the patient's inhalation, in a short time and without the need for propellers or hand-breathing coordination [12,19]. Moreover, they are handy, easy to maintain and disinfect, and can be produced as single-use inhalers to restrain the device and environmental contamination risks; which are common drawbacks of nebulizers [12].

To be formulated as dry powder for inhalation, nanoparticles (NPs) should be reversibly aggregated in the form of nano-structured or Trojan particles, that were firstly introduced by Tsapis et al. [20] and are still used until today [21–23]. The aerodynamic diameter of these particles dictates the deposition zone in the lungs. Particles exhibiting aerodynamic diameters between 0.5 and 5 μm are majorly deposited in the lower respiratory airways, where an aerodynamic diameter below 3 μm fosters alveolar deposition [12,24,25]. The nano-in-micro approach not only enables the pulmonary delivery of NPs, but also circumvents clearance by alveolar macrophages, where particles in the size range from 0.5 to 5 μm suffer extensive phagocytosis [26,27] (specifically in the range from 1.5 to 3 μm [28]). For this to be achieved, the microparticles should readily redisperse into the constituting NPs upon hydration by the pulmonary fluids. Particle redispersibility, along with surface forces, flowability, moisture content, hygroscopicity, and aerodynamic properties, necessitate the selection of matrix-forming excipients and the optimization of spray drying conditions [19].

Delivery of NPs to the alveolar region, i.e., their availability at the vicinity of the tumor masses, does not necessarily ensure the efficacy of the treatment; the NPs should penetrate into the tumor to reach the target cancer cells for releasing their load. Solid tumors are characterized by the formation of a dense extracellular matrix (ECM), which impedes the diffusion of drug molecules or nanocarriers within the tumor interstitium and hence, results in treatment inadequacies [29–32]. The ECM is composed of a highly organized network of fibrous proteins, glycoproteins, proteoglycans, glycosaminoglycans, and other macromolecules [33]. Collagen is the most abundant protein and the main structural component of the ECM [34], where fibrillar collagen type I is the most prevalent and is generally linked to tumor cell survival and metastasis in many solid tumors [35]. Intravenous or intratumoral administration of collagenase prior to treatment application has shown promising results for improving the treatment outcomes, where changes in the collagen density and/or the interstitial fluid pressure were reported [29]. More recent studies explored the nano-based delivery of collagenase through physical adsorption, direct loading, or surface chemical conjugation, revealing further ECM modulation mechanisms [32]. However, the release of collagenase with the desired kinetics and/or maintaining its enzymatic activity are potential difficulties to be tackled throughout the formulation design and evaluation steps.

Herein, our system is composed of acid-degradable acetalated maltodextrin (AcMD)-NPs embedded in a collagenase-containing water-soluble matrix, so that collagenase would be released upon the matrix dissolution in the pulmonary fluid. This would potentially enhance the penetration of the redispersed NPs into the tumor masses through the reduction of interstitial pressure. The matrix composition as well as the spray drying conditions were optimized to allow nanoparticle release and preservation of enzymatic activity. The microparticles (MPs) were characterized in terms of particle size, morphology, redispersibility, moisture content, and *in vitro* pulmonary deposition. Additionally, the acute *in vitro* cytotoxicity of the collagenase-containing MPs was tested on human lung adenocarcinoma cells (A549) and human lung fibroblasts (MRC-5). The evaluation of nanoparticle penetration was performed using a co-culture lung adenocarcinoma spheroid model consisting of A549 and MRC-5 cells.

2. Materials and methods

2.1. Materials

Maltodextrin (DE: 13.0 – 17.0), 2-methoxypropene, pyridinium *p*-toluene sulfonate (PPTS), triethylamine (TEA), 1,8-diazabicyclo[5.4.0] undec-7-ene (DBU), L-leucine, collagenase (obtained from *Clostridium histolyticum*, Type I), rhodamine B, fluorescein sodium salt, 1-octanol, RPMI-1640 cell culture medium, Dulbecco's phosphate buffered saline (DPBS), trypsin-EDTA, penicillin–streptomycin, and thiazolyl blue tetrazolium bromide were purchased from Sigma-Aldrich (Steinheim, Germany). Poloxamer 407 was purchased from Caesar and Loretz (Hilden, Germany). Trehalose was purchased from Carl Roth (Karlsruhe, Germany). NHS-Rhodamine, 4′,6-diamidino-2-phenylindole (DAPI), Gibco™ MEM α (Glutamax™ Supplement) cell culture medium, Gibco™ Opti-MEM™ serum reduced medium, and fetal bovine serum (FBS) were purchased from Thermo Fisher Scientific (Darmstadt, Germany). Dimethyl sulfoxide (DMSO, analytical grade), acetone, and ethanol (HPLC grade) were purchased from Fisher Scientific (Schwerte, Germany). *N*-hexane (HPLC grade) was purchased from VWR (Darmstadt, Germany). All the other reagents used were purchased with HPLC or analytical grade.

2.2. Preparation of AcMD-NPs

Synthesis of AcMD and rhodamine-labeled AcMD (Rhod-AcMD), and preparation of AcMD-NPs and Rhod-AcMD-NPs were adopted as described in our previous work [36]. The synthesis and preparation methods are described in the supplementary material. The yield was determined through freeze drying. A nanoparticle stock suspension of 10 mg/ml in Milli-Q water was accordingly prepared for spray drying.

2.3. Preparation of AcMD nano-structured MPs

Aqueous stock solutions of leucine (10 mg/ml) and trehalose (20 mg/ml) were prepared. Based on the required microparticle composition (**Table 1**); stock suspension of AcMD-NPs and leucine and trehalose stock solutions were mixed in different proportions and diluted with Milli-Q water. When powder quantification was required, rhodamine B was added to the spray drying feed suspension at a concentration of 50 μg for each 100 mg of total solid mass. The final total solid concentration in the precursor suspensions to be sprayed was fixed at 1 % (m/v). The nanoparticle aqueous suspension was spray dried using a Büchi Mini Spray Dryer (B-290, Büchi, Flawil, Switzerland) equipped with a standard two-fluid nozzle (0.7 mm hole diameter). Nitrogen was used as the spraying gas. The inlet temperature was adjusted to 50 °C and the resulting outlet temperature was 38 – 42 °C. The feed pump rate was set at 1.5 ml/min (5 %), the spraying gas rotameter at 50 mm (601/1052 L/h), and the aspirator at 100 % (35 m^3/h). Powder samples were collected

Table 1
Mass composition of the spray dried nano-structured MPs. The proportion of each component is expressed as the mass percentage of this component relative to the total powder mass (m%).

Sample	NP (m %)	Leucine (m %)	Trehalose (m %)	Collagenase (m %)
$NP_{20}L_{0}$*	20	0	80	0
$NP_{10}L_{30}$	10	30	60	0
$NP_{20}L_{30}$	20	30	50	0
$NP_{30}L_{30}$	30	30	40	0
$NP_{20}L_{30}C_{10}$*	20	30	40	10
$NP_{20}L_{30}C_{30}$	20	30	20	30
$NP_{20}L_{30}C_{50}$	20	30	0	50

*NP_xL_x indicates the mixing ratio of the compounds used as stated in the table: NP: fraction of AcMD-NPs, L: fraction of leucine, and C: fraction of collagenase.

and stored in a desiccator. Samples were prepared in triplicates.

For collagenase-containing samples, required amounts of collagenase were weighed and added to the rest of formulation components directly before spray drying. The formulation suspension was magnetically stirred till dissolution of collagenase and spray drying was performed as described.

2.4. Assessment of collagenase activity after spray drying

The activity of collagenase was measured colorimetrically (Collagenase Activity Colorimetric Assay Kit, Sigma-Aldrich, St. Louis, United States), following the manufacturer's protocol and using microplate reader (Infinite M200, Tecan group, Männedorf, Switzerland) in the kinetic mode. The collagenase activity was first tested against different inlet temperatures (50, 60 and 70 °C). Second, it was tested at the selected inlet temperature for different collagenase mass content per dry powder (10 %, 30 % and 50 %). It is expressed as percentage of retained activity, relative to a freshly prepared collagenase solution of an equivalent concentration to the reconstituted powder sample of interest.

2.5. Particle size and size distribution determination

Particle size and polydispersity index (PDI) of AcMD-NPs were measured using dynamic light scattering (DLS) (Zetasizer Ultra, Malvern Panalytical, Worcestershire, United Kingdom). Samples were diluted (1:100) in alkaline water and intensity-based hydrodynamic diameter was measured at 25 °C temperature and 173° angle in the back-scattering mode. The particle size of the spray-dried MPs was measured using a laser diffractometer (Master sizer 2000 Ver. 2.00, Malvern Instruments, Malvern, UK). The samples were dispersed in 1-octanol/*n*-hexane (20:80 % v/v) at a concentration of 1 mg/ml. This proportion of 1-octanol was found to produce a good dispersion of the MPs, whereas they agglomerated strongly when *n*-hexane was used solely as a dispersant. The particle suspension was added slowly to the measurement chamber under stirring till the optimum obscuration was reached. The stirring function was used at 1500 rpm. The median volume diameter ($D_{v0.5}$) and the span value were used to describe the particle size and the polydispersity, respectively. All measurements were performed in triplicates and the mean values were used.

2.6. Morphology using scanning electron microscopy (SEM) and confocal laser scanning microscopy (CLSM)

The AcMD nano-structured MPs were visualized using SEM (Zeiss EVO HD15, Carl Zeiss, Oberkochen, Germany). The powder sample was applied to silica wafers attached to a metal stub. Excess powder was air blown. The MPs were sputter coated with 10 nm gold layer (Quorum Q150R ES, Quorum Technologies, East Sussex, United Kingdom) and examined at 10 kV under high vacuum.

For the visualization of nanoparticle regional distribution within the microparticle matrix, Rhod-AcMD-NPs were used, and the matrix was labeled with sodium fluorescein. The MPs were dispersed in immersion oil (Immersol™ 518F, Carl Zeiss, Jena, Germany) and placed between two glass covers. The visualization was performed using CLSM (LSM 710, Carl Zeiss AG, Jena, Germany) using EC Plan-Neofluar 100x oil immersion objective. Fluorescein and rhodamine were excited at 488 and 561 nm using argon laser and the emission was recorded at 493 – 562 and 566 – 703 nm for each dye, respectively. Signals from both channels were merged and the images were processed using Zen 3.0 (blue edition) software (Carl Zeiss Microscopy, 2019).

2.7. Evaluation of redispersibility

2.7.1. Qualitative evaluation of redispersibility

The redispersibility was qualitatively evaluated using SEM (Zeiss EVO HD15, Carl Zeiss, Oberkochen, Germany). A thin film of powder was deposited on a silica wafer fixed on a metal stub. A volume of 10 µl of water was added on top of the powder and left for 5 min. Afterwards, the excess water was carefully wicked using Kimtech® tissue, and the sample was air dried. The MPs were sputter coated and examined as described in **section 2.6**.

2.7.2. Quantitative evaluation of redispersibility

The redispersibility was evaluated as previously described by Torge et al. [18] with minor modifications. A sample amount of approximately 10 mg (m_1) was weighed into a pre-weighed Eppendorf tube. A volume of 2 ml of simulated lung fluid (SLF 3 [37]) was added and the tubes were incubated, horizontally aligned, in a shaking water bath at 37 °C, 100 rpm for 30 min (Shaking incubator 3031, GFL, Burgwedel, Germany). Afterwards, the samples were centrifuged at 2000 g for 5 min (Sigma 3-30KS, Sigma, Osterode am Harz, Germany) to separate the redispersed NPs in the supernatant from the pelleted non-redispersed particles or fragments. The supernatants were separated, and the size and the polydispersity index (PDI) of the redispersed NPs were measured (Zetasizer Ultra, Malvern Panalytical, Worcestershire, United Kingdom). The pellets were washed by carefully adding water, and the centrifugation/washing step was repeated twice. The pellets were frozen at −80 °C and lyophilized (Alpha 2–4 LSC, Christ, Osterode am Harz, Germany), and the masses were determined after lyophilization (m_2). The redispersed powder fraction was calculated using **equation (1)**.

$$\textit{Redispersed powder fraction}(\%) = \frac{m_1 - m_2}{m_1} \times 100 \quad (1)$$

Assuming the complete dissolution of the water-soluble matrix components, the pellet was assumed to represent non-redispersed NPs. Therefore, the mass fraction of redispersed NPs was calculated by relating the redispersed nanoparticle mass to the total theoretical mass of NPs in the formulation (m_{NP}), as follows:

$$\textit{Redispersed NP fraction}(\%) = \frac{m_{NP} - m_2}{m_{NP}} \times 100 \quad (2)$$

2.8. Determination of moisture content

The moisture content was determined by thermogravimetric analysis (TGA) using a thermogravimetric analyzer (TG 209 F1 Libra, Netzsch, Selb, Germany) under nitrogen atmosphere. The analysis was carried out from 30 to 300 °C at a heating rate of 5 °C/min. The sample mass was about 5 mg, and the percentage mass loss from 30 to 150 °C was used to calculate the residual moisture content. The thermograms were generated and processed using Netzsch Proteus® Software.

2.9. Evaluation of aerodynamic properties

2.9.1. Next generation impactor (NGI) experiment

The aerodynamic properties were determined using NGI (Copley

Scientific, Nottingham, UK) [18,21,38]. A mass of approximately 10 mg of rhodamine B-labelled powder samples were weighed into hard gelatin capsules (size 3) and the capsules were securely closed. The filled capsule was placed in a HandiHaler® (Boehringer Ingelheim, Ingelheim, Germany) and punctured prior to aerosolization. The impactor cups were coated with a mixture of 15 % Brij 35 ethanolic solution and glycerol (40:60 % v/v), and the pre-separator was filled with 5 ml Milli-Q water. The gas flow was preadjusted by a flowmeter (M1A, Copley Scientific, Nottingham, UK). After the full assembly of the impactor, the inhaler was fitted at the induction port and the powder was aerosolized at 60 L/min gas flow for 4 s using a vacuum pump and critical flow controller (Erweka, Heusenstamm, Germany). The deposited powder at the induction port and the cups were collected by thorough rinsing with a definite volume of Milli-Q water. The experiment was performed in independent triplicates for all the tested formulations.

2.9.2. Powder quantification

The concentration of the deposited powder was determined through measuring the fluorescence of rhodamine B (λ_{ex}: 565 nm and λ_{em}: 625) using microplate reader (Infinite M200, Tecan group, Männedorf, Switzerland). For each powder sample, the mass of the powder collected from the induction port, the pre-separator, the stages, as well as the capsule shell, was determined against its own calibration plot in water (20 – 1000 μg/ml concentration range) and the respective cumulative powder masses were calculated.

2.9.3. Aerodynamic properties calculation

The effective cut-off diameters of the NGI stages at 60 L/min flow rate were used as specified in the European Pharmacopeia and the USP (cut-off diameters from the micro-orifice collector (MOC) to stage 1: 0.34, 0.55, 0.94, 1.66, 2.82, 4.46 and 8.06 μm in order). The cumulative powder mass percentage deposited at each stage (relative to the cumulative mass at stage 1) was calculated and transformed into probit values. The probit values were plotted against the log cut-off diameters of each stage, where a calibration range including probit of 5 and log cut-off diameter of 0.7 was used for setting the linear regression equation. The emitted dose (ED), which describes the percentage of the powder emitted from the capsule, was calculated using **equation (3)** [39]. The mass median aerodynamic diameter (MMAD) was calculated from the linear regression equation, as the diameter corresponding to the cumulative mass fraction of 50 % (probit value of 5). The geometric standard deviation (GSD) was calculated based on the 84 % (d_{84}) and 16 % (d_{16}) cut-off diameters (probit values of 5.99 and 4.01 respectively) using **equation (4)**. The fine particle fraction (FPF) was calculated using the cumulative mass fraction corresponding to cut-off diameter of 5 μm (probit value of 0.7) relative to the ED [18,40].

$$\boldsymbol{ED} = \frac{\boldsymbol{Initial\ powder\ mass - Remaining\ mass\ in\ empty\ capsules}}{\boldsymbol{Initial\ powder\ mass}} \times 100 \quad (3)$$

$$\boldsymbol{GSD} = (\boldsymbol{d}_{84}/\boldsymbol{d}_{16})^{1/2} \quad (4)$$

2.10. In vitro biological experiments

2.10.1. Cell culture

Human adenocarcinoma alveolar epithelial cells (A549) were cultured in RPMI-1640 medium supplemented with 10 % FBS. Human fetal lung fibroblasts (MRC-5) were cultured in MEM α medium with GlutaMAX™, supplemented with 10 % FBS. The cells were subcultured once a week and the media were replaced with fresh media every other day. The cultures were maintained at 37 °C in a humidified atmosphere containing 5 % CO_2 (BD 260 Standard Incubator, Binder, Tuttlingen, Germany). A549 cells were used within passages 6 and 20 and MRC-5 cells were used within passages 3 and 10.

2.10.2. Cell viability assay

The effect of AcMD nano-structured MPs on cell viability was evaluated using MTT assay on A549 and MRC-5 two dimensional (2D) cultures. A549 and MRC-5 cells were seeded into 96-well plates (20,000 and 40,000 cells/200 μl/well, respectively) and grown for 48 h. Afterwards, media were replaced with fresh media containing different concentrations of the tested MPs (100, 250, 500, 750 and 1000 μg/ml) and supplemented with 100 U/ml penicillin–streptomycin. For the negative and positive controls, the cells were treated with medium and 2 % Triton-X, respectively. After 24 h incubation, the treatments were removed, and the cells were washed with DPBS and incubated with 10 % MTT reagent for 4 h. This was followed by aspiration and incubation with DMSO for 20 min. The absorbance of formazan formed by live cells was measured at 550 nm using microplate reader (Infinite M200, Tecan group, Männedorf, Switzerland) and cell viability was calculated. The experiments were performed in triplicates.

2.10.3. Formation of spheroids

Spheroids were produced by adopting liquid overlay technique in ultra-low adhesion 96-well plates (Nuclon™ Sphera™ 96-well U-shaped-bottom microplates, Thermo Scientific). A549 monoculture as well as A549/MRC-5 co-culture spheroids were grown. The cells were seeded at 2000 cells/100 μl/well. For monoculture spheroids, the seeded cells were 100 % A549. For co-culture spheroids, the seeding ratio of A549 to MRC-5 cells was 30:70 and cell seeding was performed sequentially, where A549 cells were seeded first, followed by MRC-5 cells after 24 h [41]. The spheroids were allowed to grow for 10 days. The media were renewed by adding 100 μl fresh media at day 5 and exchanging 100 μl at day 8. For all the spheroid experiments, the media were supplemented by 100 U/ml penicillin–streptomycin. To monitor the spheroid growth, bright field images were recorded at day 2, 3, 5, 8 and 10 (LSM 710, Carl Zeiss AG, Jena, Germany) using 10x objective. Spheroid diameter was determined as the average of 3 diameters measured for each spheroid using ImageJ software. The circularity parameter was calculated by the aid of ImageJ software, based on **equation (5)** [42]. Six spheroids were examined for each experiment.

$$\boldsymbol{Circularity} = 4\pi\left(\frac{\boldsymbol{area}}{\boldsymbol{perimeter}^2}\right) \quad (5)$$

2.10.4. Application of treatments to the spheroids

After the spheroids were grown for 10 days, the spheroids were washed once with DPBS and once with Opti-MEM medium through exchanging 150 μl in each washing step. Subsequently, the microparticle components were added at a concentration of 1 mg/ml in Opti-MEM medium and incubated with the spheroids for 4 h. Subsequently, the spheroids were washed twice with Opti-MEM medium, and NPs alone were reapplied at the same concentration. Two controls were used at this experiment, a negative control in which the spheroids were treated with Opti-MEM medium (referred to as medium control), and a collagenase-negative control, in which the spheroids were treated with collagenase-free formulation. The incubation was allowed to continue till a total duration of 24 h. After incubating the spheroids with the treatments, they were washed twice with DPBS. The spheroids were fixed with 4 % paraformaldehyde for 30 min at room temperature then washed twice with DPBS. Nuclei were stained with DAPI for 1 h, followed by 2 washing steps with DPBS. In each washing and addition step, a volume of 150 μl was exchanged.

2.10.5. Effect of collagenase on the integrity of spheroids

Bright field images (LSM 710, Carl Zeiss AG, Jena, Germany) using 10x objective were recorded for the fixed spheroids, and the diameters were measured as described. To test the effect of collagenase on the integrity of spheroids, the diameter and circularity of the spheroids treated with collagenase-free and collagenase-containing formulations were compared to the medium control spheroids.

2.10.6. Evaluation of nanoparticle penetration

The spheroids were visualized with CLSM (LSM 710, Carl Zeiss AG, Jena, Germany) using 10x objective. The signals of DAPI and rhodamine were detected through excitation at 405 and 561 nm and recording emission at 410 – 507 and 566 – 703 nm, respectively. In confocal mode, the first and last planes at which cells could be observed (guided by DAPI signal) were used as the first and last visualization constraints. Through this determined depth, the rhodamine signal in 4 optical sections at equal steps (approximately 40 μm apart from each other according to the individual spheroid dimensions) was recorded. The medium control spheroids were used as a blank for setting the microscopical settings. Image processing was performed using ZEN 3.0 (blue edition) software (Carl Zeiss Microscopy, 2019). The fluorescence intensity in the consecutive planes were assessed and compared for the collagenase-free and the collagenase-containing formulations. The corrected total fluorescence (CTF) and normalized CTF were calculated using the integrated density (IntDen) and surface area (A) measured by ImageJ for the individual cross sections as follows:

$$\boldsymbol{CTF} = \boldsymbol{IntDen} - (\boldsymbol{Mean\ background\ fluorescence} \times \boldsymbol{A}) \quad (6)$$

$$\boldsymbol{Normalized\ CTF} = \frac{\boldsymbol{CTF}}{\boldsymbol{A}} \quad (7)$$

2.11. Statistical analysis

The results are described as mean values ± standard deviation of at least three independent triplicates. Statistical significance was tested using one-way analysis of variance (ANOVA), followed by the suitable *post hoc* test to compare all pairs. The level of significance was set at a *p*-value of 0.05. Statistical analysis was implemented using GraphPad Prism (version 8.0.2) software (GraphPad Software, 2019).

3. Results and discussion

3.1. Preparation of AcMD nano-structured MPs

Different excipients were preliminarily tested for the particle formation; mannitol, trehalose, and leucine, with an initial nanoparticle mass content of 10 %, feed concentration of 1 %, feed flow rate of 10 %, and inlet temperature of 70 °C. The spray-dried MPs were characterized in terms of morphology, redispersibility, and aerodynamic properties. Leucine nano-structured MPs were found to be superior in terms of redispersibility and aerodynamic properties followed by trehalose and mannitol (data not shown). However, the SEM pictures of the leucine nano-structured MPs showed relatively large, cracked particles with obvious broken fragments (**Figure S2**, supplementary material). Accordingly, a mixture of trehalose and leucine was selected for the matrix formation to enhance the mechanical strength of the particles. The spray drying conditions were also investigated by changing the feed concentration at 0.5 and 1 %, and the feed flow rate at 5 and 10 %. It was found that using 1 % feed concentration at lower flow rate yielded smaller MPs with better deposition characteristics. Leucine mass content was also tested; 30 % mass content was found sufficient for improving the redispersibility and the aerodynamic properties (data not shown). The selection of the inlet temperature and the nanoparticle mass content are addressed in the following sections.

3.2. Collagenase activity after spray drying

In order to select the optimum inlet temperature for spray drying, the activity of collagenase was assayed after spray drying at 50, 60 and 70 °C inlet temperatures. Fig. 1**a** shows that the effect of temperature in this range was minimal, with no significant difference among the inlet temperatures tested. The retained activity was as high as 89.5 ± 6.7 % when spray drying was performed at an inlet temperature of 50 °C. This result was further confirmed by spray drying formulations with increasing collagenase mass content (10 %, 30 % and 50 %), where they all exhibited comparable preservation of collagenase activity after spray drying at 50 °C (Fig. 1**b**).

Exposure to high temperatures during spray drying was supposed to pose a challenge for spray drying of collagenase, due to heat-mediated denaturation and enzyme inactivation [43]. However, the results support that spray drying is very mild, not causing a dramatic decrease in enzyme activity. This may be ascribed to the brief exposure to high temperatures, immediately followed by evaporative cooling and loss of moisture [44]. One other contributing factor is the presence of leucine and trehalose, with their protective effects due to water replacement through hydrogen bond formation [45,46]. The retainment of activity among the formulations containing increasing amounts of collagenase, and accordingly decreasing amounts of trehalose, suggests that the used amount of leucine was sufficient for enzyme activity preservation. In addition to hydrogen bond formation, orientation of hydrophobic groups of leucine towards the liquid–air interface would further protect the enzyme against denaturation [44].

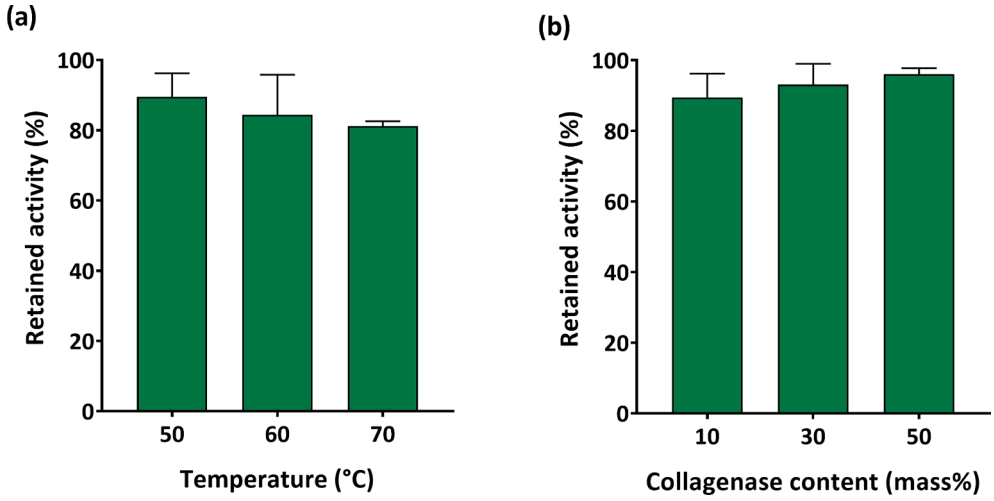

Fig. 1. Percentage of retained activity of collagenase after spray drying at (a) different inlet temperatures (50, 60 and 70 °C) and (b) increasing collagenase mass content (10 %, 30 % and 50 %). The activity was assayed by collagenase activity colorimetric kit, and the data represent mean values ± standard deviation of independent triplicates.

3.3. Particle size and size distribution

It is generally known that the smaller the particle size of the powder, the higher its potential for alveolar deposition. The particles size was found to be affected by the formulation composition (Table 2). Addition of leucine in formulations $NP_{10}L_{30}$, $NP_{20}L_{30}$ and $NP_{30}L_{30}$ was found to increase the particle size relative to the leucine-free formulation $NP_{20}L_0$. This would be attributed to the surface properties of leucine, where it accumulates at the droplet surface during the drying step forming a crust that would resist shrinkage [47]. However, changing the nanoparticle mass content from 10 % to 30 % does not appear to considerably impact the particle size distribution. Comparing collagenase-containing nano-structured MPs ($NP_{20}L_{30}C_{10}$, $NP_{20}L_{30}C_{30}$ and $NP_{20}L_{30}C_{50}$) to their collagenase-free counterpart ($NP_{20}L_{30}$), inclusion of collagenase was found to shift the particle size distribution towards smaller diameters. However, the particle diameter measured by laser diffraction does not consider the particle density nor the morphology. The MMAD is a better indication for the deposition [48], and the results of its evaluation are discussed in **section 3.7**.

3.4. Particle morphology using SEM and CLSM

The AcMD nano-structured MPs were visualized by SEM (Fig. 2). Leucine, as a formulation component, was found to have a remarkable influence on the particle size and morphology. Compared to the leucine-free $NP_{20}L_0$ (Fig. 2**a**), $NP_{20}L_{30}$ SEM images (Fig. 2**b**) show unaggregated, hollow particles with some surface corrugations and a more obvious presence of larger-sized population. This last observation conforms with the different particle size distribution detected by laser diffraction for both samples (Table 2). It is worth mentioning that surface corrugations improve the aerosol performance of the particles, where this reduces the inter-particle contact points and hence their cohesiveness and adhesiveness [48]. The presence of surface corrugations would also raise the shape factor (X), and hence decrease the aerodynamic diameter of the particles in comparison to the geometric diameter [49]. The presence of collagenase in $NP_{20}L_{30}C_{10}$, $NP_{20}L_{30}C_{30}$ and $NP_{20}L_{30}C_{50}$ (Fig. 2**c, d, and e**, respectively) does not seem to affect the particle surface morphology. Close observation of the MPs' surface reveals protruding NPs, which indicates the spatial accumulation of NPs at the surface leading to surface roughness of the nano-structured MPs. Surface roughness is assumed to positively contribute to the reduction of the inter-particulate surface forces, by increasing the distance between the adjacent particles and decreasing the area of contact [50]. The presence of leucine (with its interfacial accumulation) and NPs (with their low diffusion constant) would raise the Peclet number of the spray-dried particles, leading to the formation of those characteristic buckled, hollow particles [51], as shown in Fig. 2**b** − **e**.

Fig. 3 displays the CLSM pictures of the collagenase-free $NP_{20}L_{30}$ and the collagenase-containing $NP_{20}L_{30}C_{30}$ formulations. It can be observed that the rhodamine signal (corresponding to the AcMD-NPs) is well-defined at the periphery of the particles, in contrast to the fluorescein signal (corresponding to the matrix) that appears to be more diffuse. This indicates the surface accumulation and distribution of the AcMD-NPs which could not be concluded solely by the SEM images. The shapes exhibited by the matrix-localized fluorescein signal additionally confirm the hollowness of the MPs.

Table 2
Particle size distribution of spray-dried nano-structured MPs. The results show 10, 50 and 90 percentile volume diameters ($D_{v0.1}$, $D_{v0.5}$ and $D_{v0.9}$, respectively) and the Span index. The displayed results represent the mean ± standard deviation of three independent volume-based light scattering measurements.

Sample	$D_{v0.1}$ (μm)	$D_{v0.5}$ (μm)	$D_{v0.9}$ (μm)	Span
$NP_{20}L_0$	0.56 ± 0.13	1.67 ± 0.19	5.70 ± 0.75	3.08 ± 0.17
$NP_{10}L_{30}$	0.68 ± 0.05	6.55 ± 0.54	13.03 ± 0.25	1.89 ± 0.12
$NP_{20}L_{30}$	0.61 ± 0.01	6.82 ± 0.61	11.89 ± 1.12	1.65 ± 0.02
$NP_{30}L_{30}$	0.51 ± 0.11	4.43 ± 0.72	9.40 ± 0.07	2.04 ± 0.32
$NP_{20}L_{30}C_{10}$	0.41 ± 0.04	2.99 ± 0.54	8.48 ± 1.9	2.67 ± 0.31
$NP_{20}L_{30}C_{30}$	0.35 ± 0.04	2.58 ± 1.35	7.14 ± 1.47	2.89 ± 0.73
$NP_{20}L_{30}C_{50}$	0.33 ± 0.02	3.01 ± 0.68	8.03 ± 0.91	2.81 ± 0.81

3.5. Redispersibility evaluation

Sufficient redispersibility of MPs into NPs in SLF is a prerequisite, so that the effects and benefits of the latter could be realized. Fig. 4 shows the morphology of redispersed particles after hydration of MPs for 5 min. It could be observed from the SEM pictures that the fully redispersed NPs are well separated with no major aggregation and comparable morphology to the NPs before spray drying (**Figure S1**, supplementary material).

The influence of nanoparticle mass content was first investigated by increasing it at 10, 20 and 30 % in formulations $NP_{10}L_{30}$, $NP_{20}L_{30}$ and $NP_{30}L_{30}$, respectively. While increasing the nanoparticle content from 10 % to 20 % did not affect the redispersed powder fraction significantly, increasing it further to 30 % lead to a significant decrease in redispersed powder fraction (Fig. 5**a**). The positive effect of leucine on the redispersibility could be clearly observed by comparing $NP_{20}L_{30}$ to its leucine-blank analogue, $NP_{20}L_0$ (Fig. 5**a**). Both the redispersed powder and nanoparticle fractions were significantly improved by the addition of leucine, where they reached 91.6 ± 0.4 % and 58.1 ± 1.8 %, respectively, for the leucine- containing formulation, $NP_{20}L_{30}$. Introducing collagenase to the best redispersing formulation, $NP_{20}L_{30}$ maintained its redispersibility attributes and showed slightly improved redispersability, with no significant differences among the individual formulations $NP_{20}L_{30}C_{10}$, $NP_{20}L_{30}C_{30}$ and $NP_{20}L_{30}C_{50}$ (with increasing collagenase mass content at 10 %, 30 % and 50 %). Fig. 5**b** shows that except for $NP_{20}L_0$, the redispersed NPs from all the investigated samples exhibited comparable particle size distribution to that before spray drying, with slightly increased diameters and acceptable polydispersity.

3.6. Moisture content

The moisture content of the spray-dried collagenase-free ($NP_{20}L_{30}$) and collagenase-containing ($NP_{20}L_{30}C_{10}$, $NP_{20}L_{30}C_{30}$ and $NP_{20}L_{30}C_{50}$) formulations ranged from 2.03 ± 0.50 % to 3.10 ± 0.20 % (Table 3). A residual moisture content of less than 5 % is sufficiently low to protect the particles against polymorphic changes, crystal formation and growth, and changes in particle size distribution upon storage [47,48,52]. Additionally, the residual moisture content should be as low as possible not only to avoid the pre-mentioned changes, but also to preserve collagenase from inactivation. Although the spray drier was operated at a relatively low inlet temperature of 50 °C, the obtained low moisture content shows the positive impact of the utilized low feed rate and maximal aspiration on the efficiency of moisture elimination. Moreover, the formation of a hydrophobic outer shell layer due to the presence of leucine is assumed to have an anti-hygroscopic effect and enhance the physical and chemical stability of the particles [47,53,54].

3.7. Aerodynamic properties

For alveolar pulmonary deposition, the powder should have a MMAD below 3 μm [17]. Table 3 depicts that the MMAD of all the investigated powder formulations was within the required limit, with an acceptable distribution around the MMAD (GSD of around 2 is acceptable for specific deposition in a certain region of the lungs [55]), which supports the feasibility of the prepared formulations. The FPF, which describes the amount of the powder that reaches the deep lungs, approached 70 % for the collagenase-containing formulations ($NP_{20}L_{30}C_{10}$, $NP_{20}L_{30}C_{30}$ and $NP_{20}L_{30}C_{50}$). It could be noted that the FPF of the collagenase-free formulation ($NP_{20}L_{30}$) is lower than the collagenase-containing counterparts. This can be related to the larger particle size of the powder as was shown by the laser diffraction measurements, which is reflected by

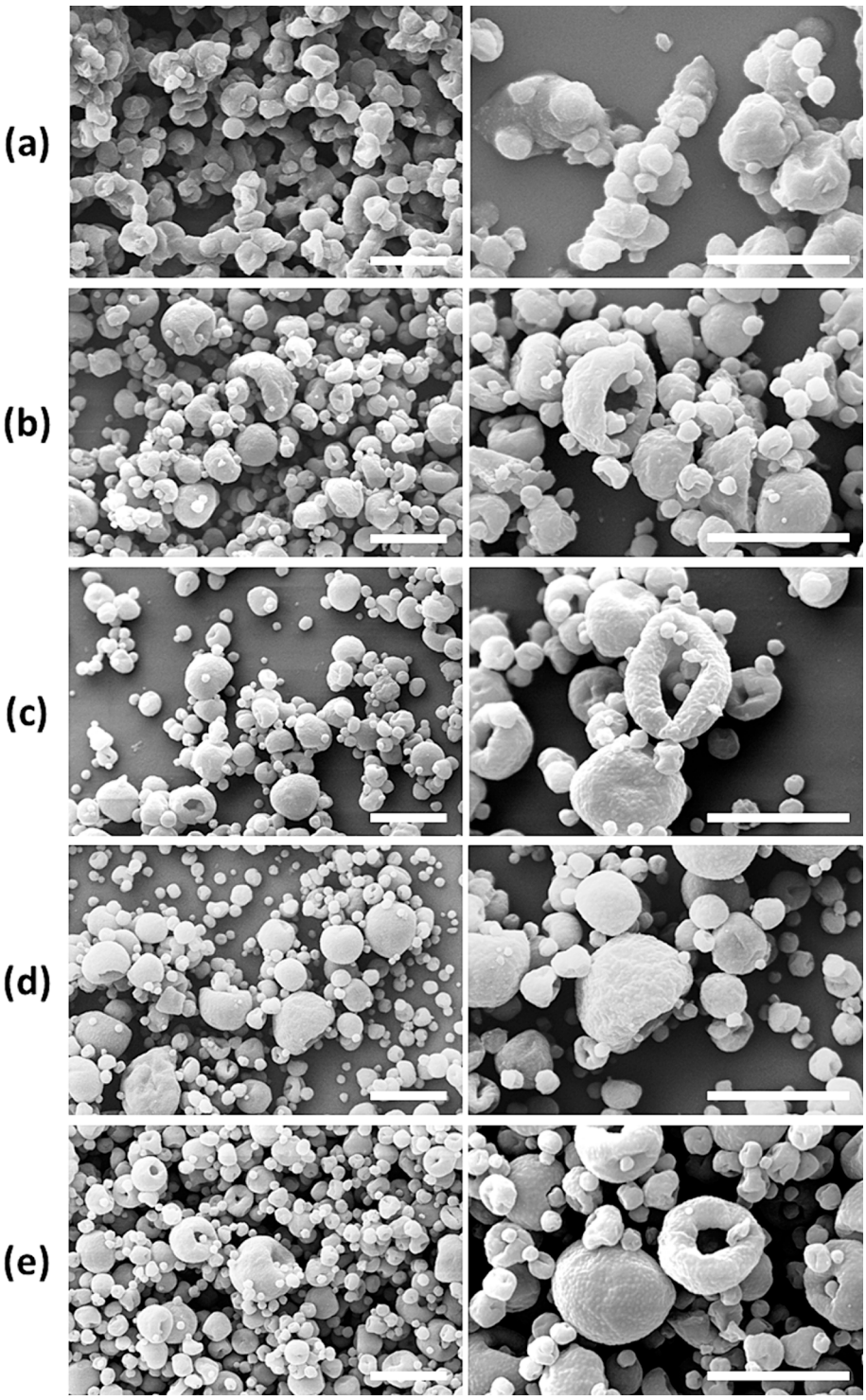

Fig. 2. SEM pictures of (a) $NP_{20}L_0$, (b) $NP_{20}L_{30}$, (c) $NP_{20}L_{30}C_{10}$, (d) $NP_{20}L_{30}C_{30}$ and (e) $NP_{20}L_{30}C_{50}$ powder samples. Right panel images were captured at higher magnification (20,000x) relative to left panel images (10,000x). Scale bars are equivalent to 5 μm.

the relatively larger GSD of $NP_{20}L_{30}$. The high ED measured for all the formulations indicates sufficiently minimal adhesive forces between the powder and the capsule.

3.8. *In vitro biological experiments*

3.8.1. *Cell viability assay*

The effect of AcMD nano-structured MPs containing increasing amounts of collagenase ($NP_{20}L_{30}C_{10}$, $NP_{20}L_{30}C_{30}$ and $NP_{20}L_{30}C_{50}$) on the viability of the two cell lines used in this study, A549 and MRC-5 cells, was tested using MTT viability assay on 2D monocultures. Similar to the collagenase-free AcMD nano-structured MPs ($NP_{20}L_{30}$), $NP_{20}L_{30}C_{10}$ even at high concentrations did not show signs of cytotoxicity for both tested cell lines (Fig. 6**)**. However, increasing the collagenase content to 30 % caused the viable fraction of MRC-5 cells to drop below 80 % at 1000 μg/ml concentration **(**Fig. 6**b)**, where a viability of 80 % is often considered as the lower limit for claiming non-cytotoxicity [56]. Further, $NP_{20}L_{30}C_{50}$ was toxic to both cell lines at concentrations higher

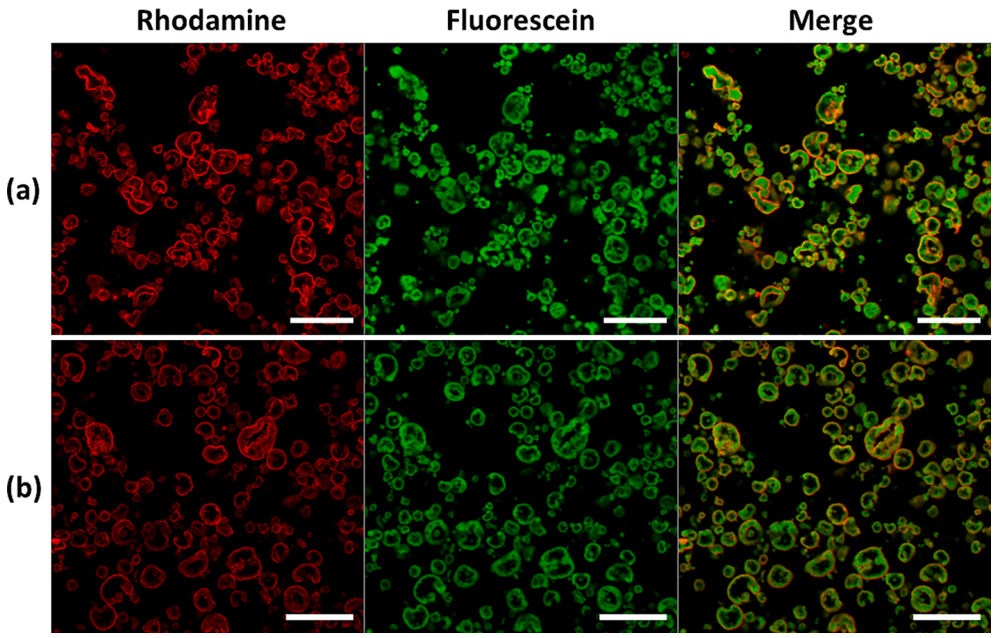

Fig. 3. CLSM pictures of (a) $NP_{20}L_{30}$ and (b) $NP_{20}L_{30}C_{30}$ nano-structured MPs showing the distribution of the NPs within the MPs' matrix. Rhodamine and fluorescein signals correspond to Rhod-AcMD-NPs and microparticle matrix, respectively. Scale bars represent 10 μm.

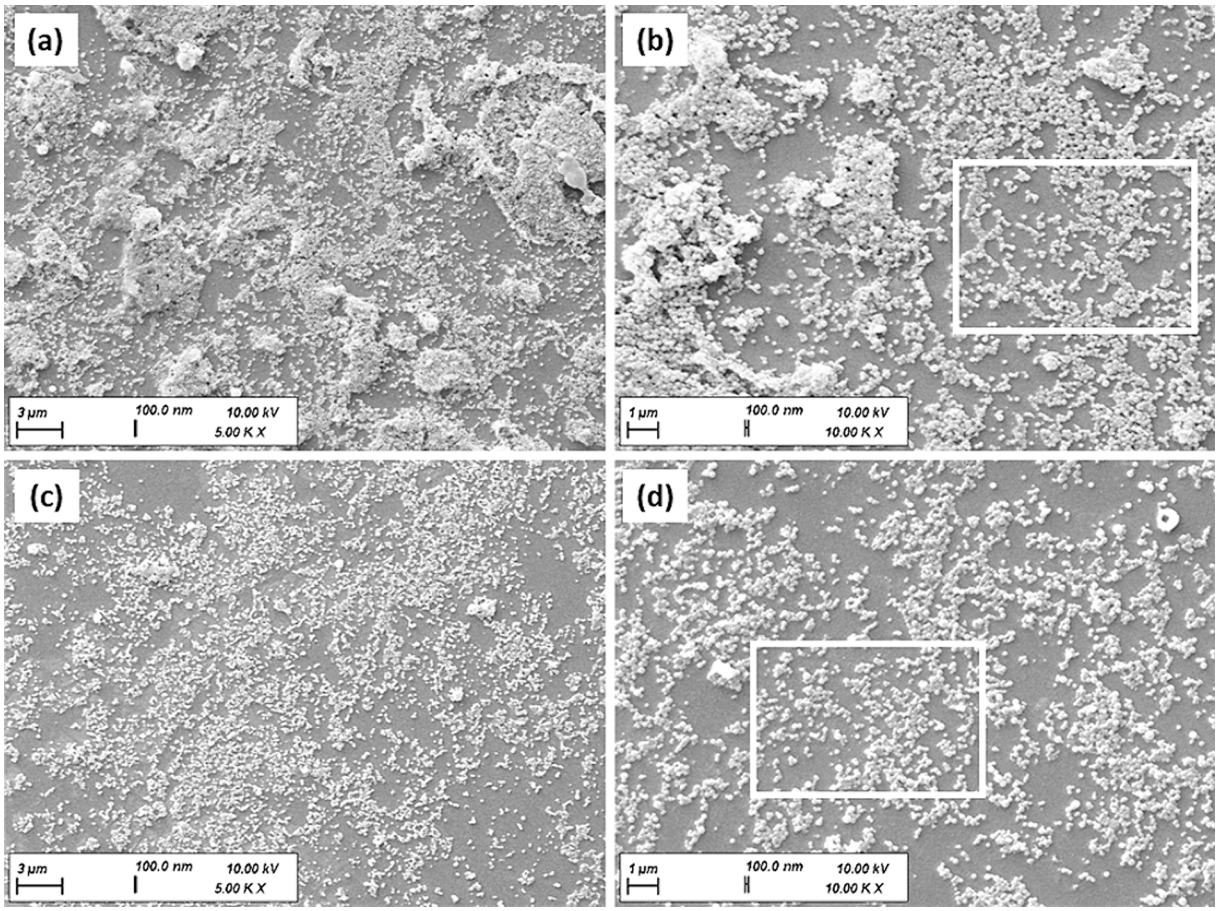

Fig. 4. $NP_{20}L_{30}$ (a and b) and $NP_{20}L_{30}C_{30}$ (c and d) redispersed MPs after hydration with water for 5 min. The magnification power of the images (a and c) is 5,000x and that of the images (b and d) is 10,000x. Well-defined NPs could be clearly seen for both powder samples (redispersed NPs as in the indicated frames for instance) with some aggregates of not fully redispersed particles.

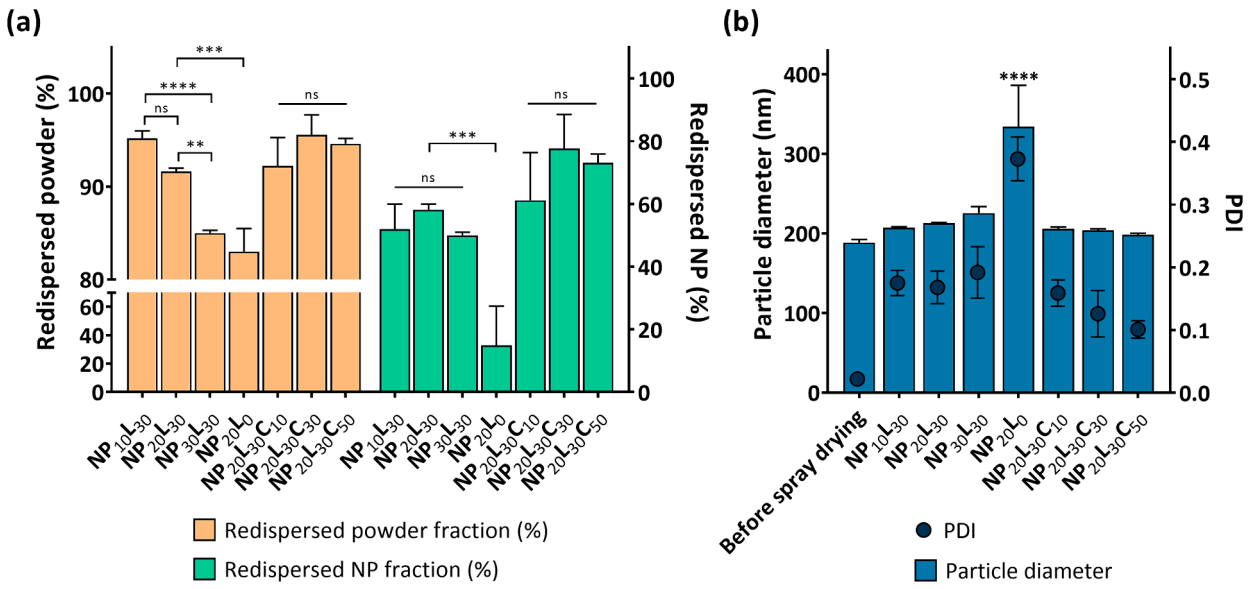

Fig. 5. (a) Redispersed powder and nanoparticle percentages after dispersion of the tested MPs in SLF. MPs containing increasing content of NPs ($NP_{10}L_{30}$, $NP_{20}L_{30}$ and $NP_{30}L_{30}$), increasing amount of collagenase ($NP_{20}L_{30}C_{10}$, $NP_{20}L_{30}C_{30}$ and $NP_{20}L_{30}C_{50}$), as well as leucine-free MPs ($NP_{20}L_0$) were tested. (b) Particle diameter and PDI of NPs released after microparticle dispersion in SLF compared to particle size and PDI of AcMD-NPs before spray drying. The results represent mean ± standard deviation of independent triplicates. Multiple comparison was performed using Tukey or Dunnett *post hoc* tests between all the pairs or with respect to standard sample, respectively. ****: $p < 0.0001$, ***: $p < 0.001$, **: $p < 0.01$ and ns: $p > 0.05$.

Table 3
Moisture content and aerodynamic properties (ED, MMAD, GSD and FPF) of spray dried collagenase-free ($NP_{20}L_{30}$) and collagenase-containing ($NP_{20}L_{30}C_{10}$, $NP_{20}L_{30}C_{30}$ and $NP_{20}L_{30}C_{50}$) powder samples. The moisture content was determined using TGA analysis. The aerodynamic properties were evaluated using NGI. The results represent mean ± standard deviation of independent triplicates.

Sample	Moisture content (%)	ED (%)	MMAD (μm)	GSD (μm)	FPF (%)
$NP_{20}L_{30}$	2.03 ± 0.50	96.33 ± 1.01	2.22 ± 0.28	2.36 ± 0.33	60.59 ± 4.72
$NP_{20}L_{30}C_{10}$	2.71 ± 0.17	94.35 ± 0.32	1.93 ± 0.06	2.19 ± 0.03	69.62 ± 2.01
$NP_{20}L_{30}C_{30}$	3.01 ± 0.20	94.90 ± 1.11	2.80 ± 0.10	1.78 ± 0.02	68.79 ± 4.80
$NP_{20}L_{30}C_{50}$	3.10 ± 0.20	92.20 ± 3.76	2.72 ± 0.39	1.79 ± 0.02	68.02 ± 6.86

than 500 μg/ml (**Fig. 6a and b**). Aside from collagenase, the MPs' constituents, including the AcMD-NPs [36], are not assumed to induce cell toxicity. Collagenase was reported to induce toxicities in animals at doses exceeding 500 μg [57,58]. To maximize the amount of the delivered AcMD-NPs, the formulation with the lowest collagenase content ($NP_{20}L_{30}C_{10}$) with the highest application concentration (1000 μg /ml) was selected for subsequent testing.

3.8.2. Spheroid formation and growth

Different seeding densities (from 1000 to 4000 cells/100 μl/well) were tested (data not shown) and 2000 cells/100 μl/well was found suitable to produce the required spheroids with diameters exceeding 500 μm at 10th day of growth. Spheroids of diameters larger than 500 μm are generally regarded as representative models for solid tumors, exhibiting their characteristic proliferation gradients of a central necrotic core, surrounded by viable quiescent cells, and finally proliferating cells at the periphery [59]. Co-culturing the fibroblasts at 70 % (compared to 50 % and 90 %) of the seeded cells was also found to yield a good compromise regarding the growth rate and circularity (data not shown), where the circularity was set as an indicator for the spheroid compactness [60].

The influence of the MRC-5 fibroblasts on the spheroid development can be clearly observed in Fig. 7. At the second day of growth prior to the addition of fibroblasts, a loose cell aggregation with undefined shape

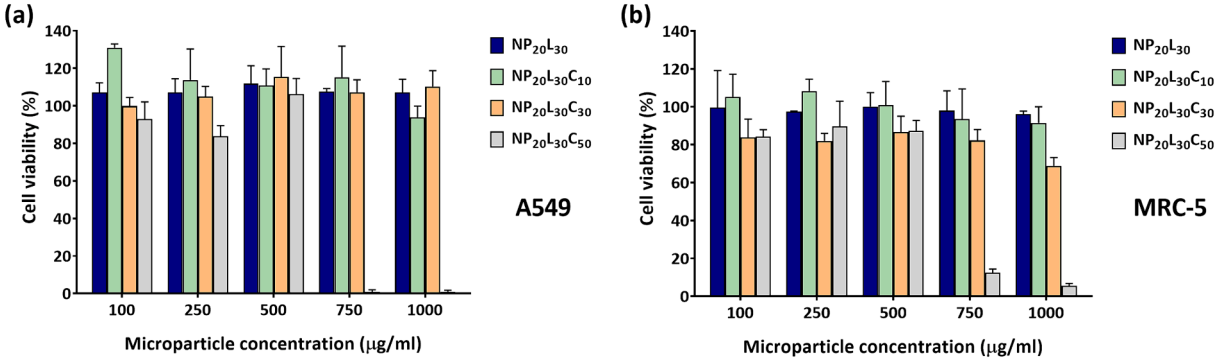

Fig. 6. Cell viability of (a) A549 cells and (b) MRC-5 fibroblasts after 24 h incubation with $NP_{20}L_{30}$, $NP_{20}L_{30}C_{10}$, $NP_{20}L_{30}C_{30}$ and $NP_{20}L_{30}C_{50}$ spray-dried nanostructured MPs at increasing concentrations (100 – 1000 μg/ml), determined using MTT assay. The data represent mean values ± standard deviation from 3 independent experiments.

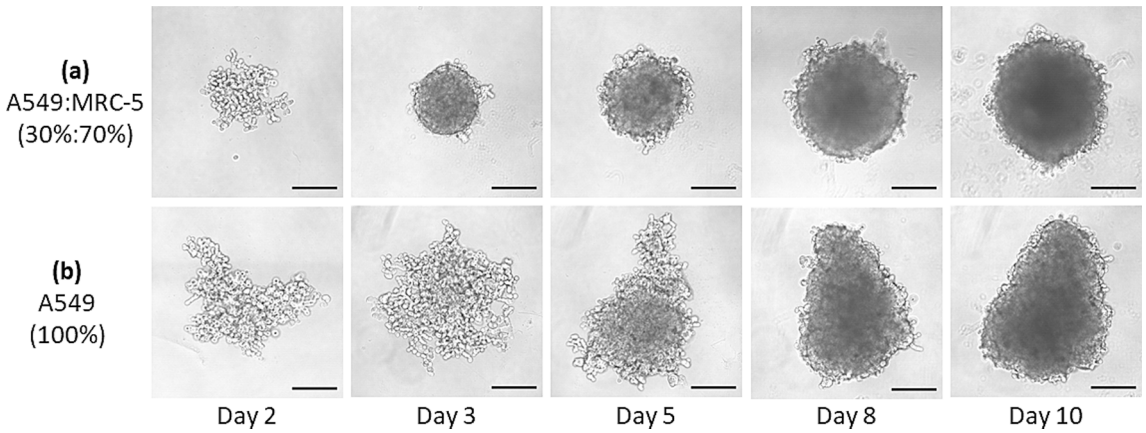

Fig. 7. Bright field images of (a) A549/MRC-5 (30 %:70 %) and (b) A549 (100 %) spheroids on day 2, 3, 5, 8 and 10 of spheroid growth. Scale bar in all pictures equals 200 μm.

was detected (Fig. 7**a**). The spheroid morphology was eminently altered by the addition of fibroblasts; the loose aggregates were transformed into tight and perfectly spherical spheroids at the third day of growth (Fig. 7**a**), displaying a gradual increase in diameter (Fig. 8**a**) and yet a preserved circular shape (Fig. 8**b**). The development pattern of the A549 monoculture spheroids was dissimilar to that of the co-culture spheroids (Fig. 7**b**). Loose, large, and irregular-shaped aggregates were initially formed, that gradually got denser and tighter over the growth period, with a less notable increase in diameter (Fig. 8**a**) and an improving circularity (Fig. 8**b**). As a whole, the results depicts the impact of cell type, seeding and culturing conditions on the characteristics of the produced spheroids [42,61].

3.8.3. *Effect of collagenase on spheroid integrity*

Based on the cell viability testing, it was concluded that applying $NP_{20}L_{30}C_{10}$ at 1 mg/ml concentration (effective concentration of collagenase is 0.1 mg/ml) was well tolerated by both A549 and MRC-5 cells. However, the effect of the ECM-degrading collagenase on the architecture of the spheroids is an additional concern, where considerable detachment of cancer cells from the spheroid surface may correspond to the initiation of metastasis [29]. Therefore, we evaluated the application of collagenase at 0.1 as well as 0.05 mg/ml concentrations (denoted as $NP_{20}L_{30}C_{10}$ and $NP_{20}L_{30}C_{05}$ respectively). Fig. 9**a** shows that the two tested collagenase concentrations caused a slight decrease in the spheroid diameter, which was statistically significant in case of the higher concentration. The significant change in circularity in case of the higher concentration (Fig. 9**b**) also implies a certain degree of deformation due to cell loosening or separation. The effects encountered may also be ascribed to the periphery of the spheroids being less rich in fibroblasts and hence in ECM, i.e., more prone to collagenase treatment. Although sequential seeding was carried out to circumvent this problem, it is speculated to improve the fibroblasts distribution only to a certain extent and render it more homogenous. Nevertheless, the lower collagenase concentration was regarded as apt to apply on the spheroids with no significant degenerating effects.

3.8.4. *Evaluation of particle penetration*

Fig. 10 demonstrates that nanoparticle fluorescence detected in the z-stack planes was more intense in case of the combined treatment of collagenase with Rhod-AcMD-NPs relative to the sole nanoparticle application (more obvious in the middle planes). This qualitative result was verified by the quantitative measurement of the fluorescent intensity of the sections, of which the results are displayed in Fig. 11. Despite the comparable fluorescence in the outer-most plane, collagenase could effectively increase the penetration of Rhod-AcMD-NPs through the spheroids to reach a depth of 120 μm. The outer-most layer is mainly comprised of actively proliferating cells and hence the particles could have been included or uptaken during cell division. The last examined plane (innermost) showed more fluorescence in the collagenase-treated sample, but the difference was not significant between the two treatments, which may be as well ascribed to the limited visualization ability of CLSM in deeper tissue sections [62].

4. Conclusion

Spray drying of AcMD-NPs into inhalable nano-structured MPs using a combination of water-soluble matrix forming agents; trehalose and leucine, was successfully realized. The formulation composition and process parameters were optimized to yield particles exhibiting three main essential features: (i) the desired aerodynamic properties to reach

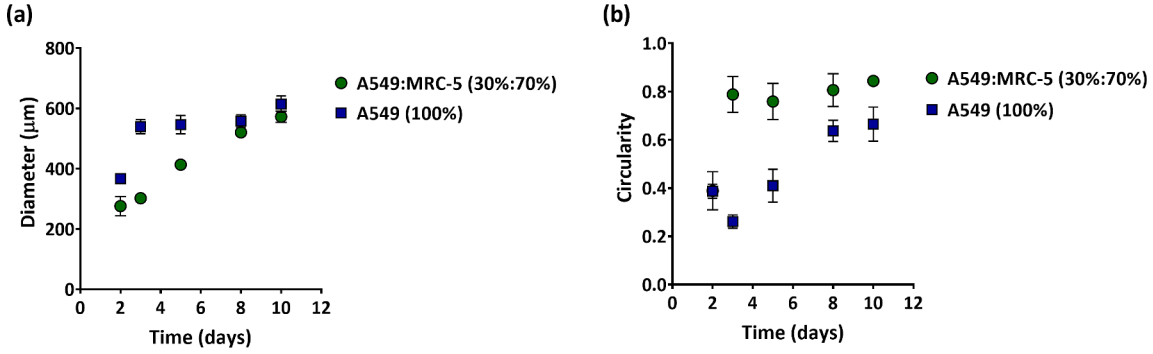

Fig. 8. (a) Diameter and (b) circularity of co-culture (A549/MRC-5) and monoculture (A549) spheroids over 10 days of spheroid growth. The results represent mean ± standard deviation of 6 independent replicates.

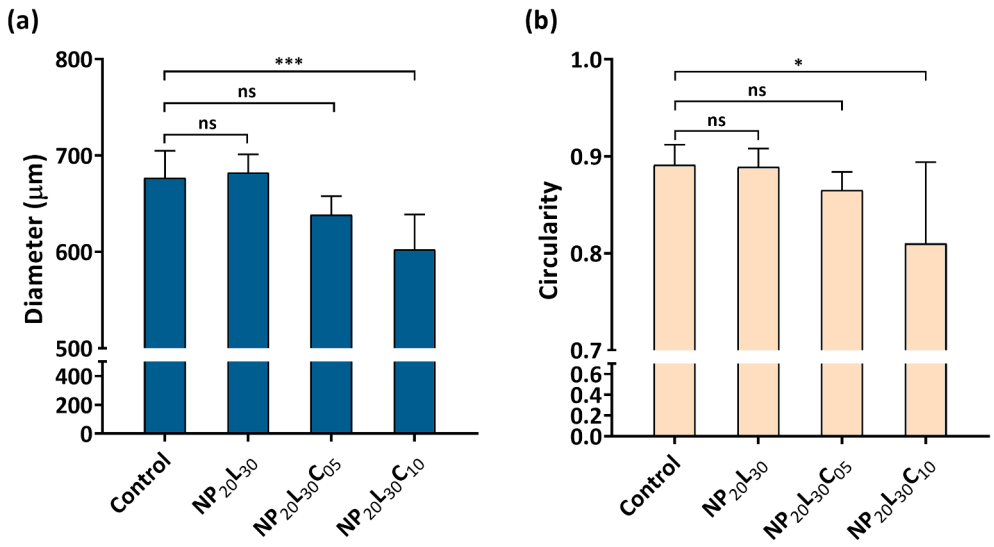

Fig. 9. (a) Diameter and (b) circularity of the spheroids after incubation with collagenase-free ($NP_{20}L_{30}$) and collagenase-containing ($NP_{20}L_{30}C_{05}$ and $NP_{20}L_{30}C_{10}$) formulation constituents relative to untreated control spheroids. The results represent mean ± standard deviation of 6 independent replicates. The respective pairs were compared using Bonferroni *post hoc* test. ***: $p = 0.0003$, *: $p = 0.0171$ and ns: $p > 0.05$.

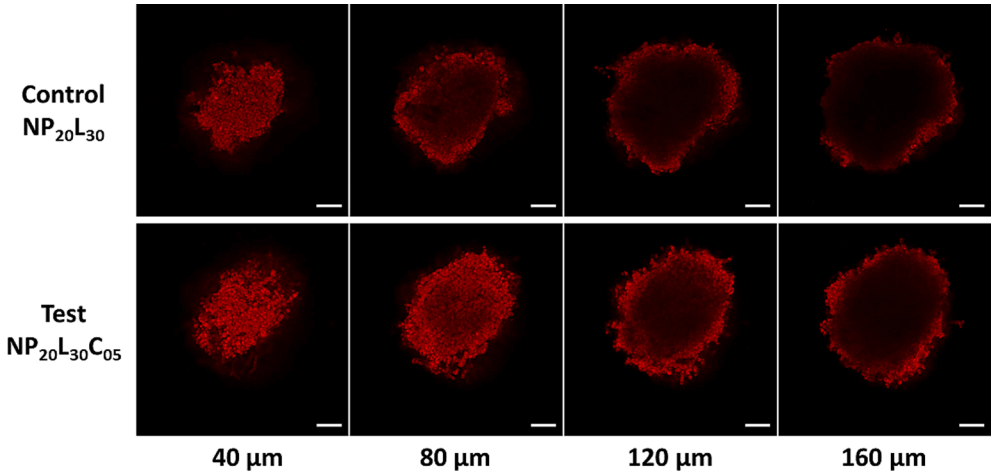

Fig. 10. Z-stack images of successive optical sections recorded at ≈ 40 μm steps. Upper and lower panels display sections of spheroids treated with $NP_{20}L_{30}$ (collagenase-free) and $NP_{20}L_{30}C_{05}$ (collagenase-containing) formulation components, respectively. Red signal corresponds to Rhod-AcMD-NPs. Scale bars are equivalent to 200 μm. (For interpretation of the references to colour in this figure legend, the reader is referred to the web version of this article.)

the alveolar region, (ii) sufficient redispersibility into NPs upon hydration, and (iii) non-impaired collagenase activity after spray drying. The inclusion of collagenase in the nano-structured microparticle formulation was depicted to enhance the penetration of AcMD-NPs into the utilized spheroid model. In other words, our proposed formulation strategy enabled the delivery of a higher amount of AcMD-NPs into deeper areas of the spheroids. Considering that the tested AcMD-NPs are relatively large (≈ 170 – 180 nm), the penetration could probably be further improved by decreasing the particle size of the embedded NPs. Interestingly, partial degradation of AcMD-NPs in acidic tumor microenvironment (TME) may result in decreasing their particle size and improving their diffusion through the ECM network. However, premature extracellular drug release should be avoided, which demands further formulation optimization and biological evaluation. The design of the carrier system introduced in this work opens several pathways for future studies investigating therapeutics effects. The dual enhancing impact of ECM modulation and nanoparticle acid-degradability on the delivery efficacy of chemotherapeutics would potentially attain the anticipated treatment outcomes.

Funding

Salma M. Abdel-Hafez was supported by a PhD scholarship (91705725) within the German Egyptian Research Long-Term Scholarship (GERLS) Program, co-funded by the German Academic Exchange Service (DAAD) and the Egyptian Ministry of Higher Education.

CRediT authorship contribution statement

Salma M. Abdel-Hafez: Investigation, Methodology, Writing – original draft, Writing – review & editing. **Markus Gallei:** Supervision, Writing – review & editing. **Sylvia Wagner:** Supervision, Writing – review & editing. **Marc Schneider:** Conceptualization, Methodology, Supervision, Writing – review & editing.

Declaration of competing interest

The authors declare that they have no known competing financial interests or personal relationships that could have appeared to influence

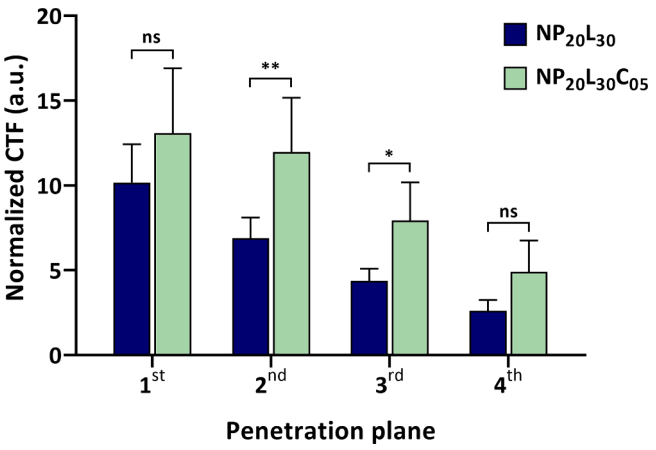

Fig. 11. The normalized CTF recorded from the different planes of spheroids ranging from 40 to 160 μm depth after incubation with $NP_{20}L_{30}$ (collagenase-free) and $NP_{20}L_{30}C_{05}$ (collagenase-containing) formulation constituents. The results represent mean ± standard deviation of 6 independent replicates. The respective pairs were compared using Bonferroni *post hoc* test. **: $p = 0.0014$, *: $p = 0.0386$ and ns: $p > 0.05$.

the work reported in this paper.

Data availability

Data will be made available on request.

Acknowledgement

The authors would like to thank Dr. Michelle Müller (Department Bioprocessing and Bioanalytics, Fraunhofer Institute for Biomedical Engineering IBMT) for her assistance and remarks about the development and characterization of spheroid models, Marijas Jurisic (Biopharmaceutics and Pharmaceutical Technology, Saarland University) for his help with the biological experiments, and Blandine Boßmann (Polymer Chemistry, Saarland University) for her technical assistance with the TGA measurements.

Appendix A. Supplementary data

Supplementary data to this article can be found online at https://doi.org/10.1016/j.ejpb.2024.114512.

References

[1] J. Ferlay, M. Colombet, I. Soerjomataram, D.M. Parkin, M. Piñeros, A. Znaor, F. Bray, Cancer statistics for the year 2020: an overview, Int. J. Cancer 149 (2021) 778–789.
[2] H. Sung, J. Ferlay, R.L. Siegel, M. Laversanne, I. Soerjomataram, A. Jemal, F. Bray, Global cancer statistics 2020: GLOBOCAN estimates of incidence and mortality worldwide for 36 cancers in 185 countries, CA Cancer J. Clin. 71 (2021) 209–249.
[3] K. Inamura, Lung cancer: understanding its molecular pathology and the 2015 WHO classification, Front Oncol 7 (2017) 193.
[4] S. Blandin Knight, P.A. Crosbie, H. Balata, J. Chudziak, T. Hussell, C. Dive, Progress and prospects of early detection in lung cancer, Open Biol. 7 (2017).
[5] N. Duma, R. Santana-Davila, J.R. Molina, Non-small cell lung cancer: epidemiology, screening, diagnosis, and treatment, Mayo Clin. Proc. 94 (2019) 1623–1640.
[6] Z. Khodabakhshi, S. Mostafaei, H. Arabi, M. Oveisi, I. Shiri, H. Zaidi, Non-small cell lung carcinoma histopathological subtype phenotyping using high-dimensional multinomial multiclass CT radiomics signature, Comput. Biol. Med. 136 (2021) 104752.
[7] M.G. Raso, N. Bota-Rabassedas, I.I. Wistuba, Pathology and classification of SCLC, Cancers 13 (2021).
[8] M. Zheng, Classification and pathology of lung cancer, Surg. Oncol. Clin. N. Am. 25 (2016) 447–468.
[9] N. Alhajj, C.F. Chee, T.W. Wong, N.A. Rahman, N.H. Abu Kasim, P. Colombo, Lung cancer: active therapeutic targeting and inhalational nanoproduct design, Expert Opin. Drug Deliv. 15 (2018) 1223–1247.
[10] C. Zappa, S.A. Mousa, Non-small cell lung cancer: current treatment and future advances, Translational Lung Cancer Research 5 (2016) 288–300.
[11] H. Lemjabbar-Alaoui, O.U.I. Hassan, Y.-W. Yang, P. Buchanan, Lung cancer: Biology and treatment options, Biochimica et Biophysica Acta (BBA) - Reviews on Cancer 1856 (2015) 189–210.
[12] R. Rosière, K. Amighi, N. Wauthoz, Chapter 10 - nanomedicine-based inhalation treatments for lung cancer, in: P. Kesharwani (Ed.) Nanotechnology-Based Targeted Drug Delivery Systems for Lung Cancer, Academic Press 2019, pp. 249-268.
[13] F. Gagnadoux, J. Hureaux, L. Vecellio, T. Urban, A. Le Pape, I. Valo, J. Montharu, V. Leblond, M. Boisdron-Celle, S. Lerondel, C. Majoral, P. Diot, J.L. Racineux, E. Lemarie, Aerosolized chemotherapy, J Aerosol Med Pulm Drug Deliv 21 (2008) 61–70.
[14] H.M. Abdelaziz, M. Gaber, M.M. Abd-Elwakil, M.T. Mabrouk, M.M. Elgohary, N. M. Kamel, D.M. Kabary, M.S. Freag, M.W. Samaha, S.M. Mortada, K.A. Elkhodairy, J.Y. Fang, A.O. Elzoghby, Inhalable particulate drug delivery systems for lung cancer therapy: nanoparticles, microparticles, nanocomposites and nanoaggregates, J. Control. Release 269 (2018) 374–392.
[15] H.M. Mansour, Y.S. Rhee, X. Wu, Nanomedicine in pulmonary delivery, Int. J. Nanomed. 4 (2009) 299–319.
[16] J.C. Sung, B.L. Pulliam, D.A. Edwards, Nanoparticles for drug delivery to the lungs, Trends Biotechnol. 25 (2007) 563–570.
[17] M. Ibrahim, R. Verma, L. Garcia-Contreras, Inhalation drug delivery devices: technology update, Medical devices (Auckland, N.Z.), 8 (2015) 131-139.
[18] A. Torge, P. Grützmacher, F. Mücklich, M. Schneider, The influence of mannitol on morphology and disintegration of spray-dried nano-embedded microparticles, Eur. J. Pharm. Sci. 104 (2017) 171–179.
[19] N. Alhajj, N.J. O'Reilly, H. Cathcart, Designing enhanced spray dried particles for inhalation: a review of the impact of excipients and processing parameters on particle properties, Powder Technol. 384 (2021) 313–331.
[20] N. Tsapis, D. Bennett, B. Jackson, D.A. Weitz, D.A. Edwards, Trojan particles: large porous carriers of nanoparticles for drug delivery, Proceedings of the National Academy of Sciences of the United States of America, 99 (2002) 12001-12005.
[21] N. Lababidi, E. Ofosu Kissi, W.A.M. Elgaher, V. Sigal, J. Haupenthal, B.C. Schwarz, A.K.H. Hirsch, T. Rades, M. Schneider, Spray-drying of inhalable, multifunctional formulations for the treatment of biofilms formed in cystic fibrosis, J. Control. Release 314 (2019) 62–71.
[22] E. Preis, E. Baghdan, M.R. Agel, T. Anders, M. Pourasghar, M. Schneider, U. Bakowsky, Spray dried curcumin loaded nanoparticles for antimicrobial photodynamic therapy, Eur. J. Pharm. Biopharm. 142 (2019) 531–539.
[23] G. Costabile, E. Mitidieri, D. Visaggio, R. Provenzano, A. Miro, F. Quaglia, I. d'Angelo, E. Frangipani, R. Sorrentino, P. Visca, R. d'Emmanuele di Villa Bianca, F. Ungaro, Boosting lung accumulation of gallium with inhalable nano-embedded microparticles for the treatment of bacterial pneumonia, Int. J. Pharm. 629 (2022) 122400.
[24] J. Heyder, Deposition of inhaled particles in the human respiratory tract and consequences for regional targeting in respiratory drug delivery, Proc. Am. Thorac. Soc. 1 (2004) 315–320.
[25] B. Chaurasiya, Y.Y. Zhao, Dry powder for pulmonary delivery: a comprehensive review, Pharmaceutics 13 (2020).
[26] C.A. Ruge, J. Kirch, C.-M. Lehr, Pulmonary drug delivery: from generating aerosols to overcoming biological barriers—therapeutic possibilities and technological challenges, Lancet Respir. Med. 1 (2013) 402–413.
[27] H.I. Shahin, L. Chablani, A comprehensive overview of dry powder inhalers for pulmonary drug delivery: challenges, advances, optimization techniques, and applications, J. Drug Delivery Sci. Technol. 84 (2023) 104553.
[28] B. Olsson, E. Bondesson, L. Borgström, S. Edsbäcker, S. Eirefelt, K. Ekelund, L. Gustavsson, T. Hegelund-Myrbäck, Pulmonary Drug Metabolism, Clearance, and Absorption, in: H.D.C. Smyth, A.J. Hickey (Eds.), Controlled Pulmonary Drug Delivery, Springer, New York, NY, 2011, pp. 21–50.
[29] A. Dolor, F.C. Szoka Jr., Digesting a path forward: the utility of collagenase tumor treatment for improved drug delivery, Mol. Pharm. 15 (2018) 2069–2083.
[30] Z. Zhao, A. Ukidve, J. Kim, S. Mitragotri, Targeting strategies for tissue-specific drug delivery, Cell 181 (2020) 151–167.
[31] J. Huang, L. Zhang, D. Wan, L. Zhou, S. Zheng, S. Lin, Y. Qiao, Extracellular matrix and its therapeutic potential for cancer treatment, Signal Transduct. Target. Ther. 6 (2021) 153.
[32] X. Xu, Y. Wu, X. Qian, Y. Wang, J. Wang, J. Li, Y. Li, Z. Zhang, Nanomedicine strategies to circumvent intratumor extracellular matrix barriers for cancer therapy, Adv. Healthc. Mater. 11 (2022) 2101428.
[33] K.C. Valkenburg, A.E. de Groot, K.J. Pienta, Targeting the tumour stroma to improve cancer therapy, Nat. Rev. Clin. Oncol. 15 (2018) 366–381.
[34] T.R. Cox, The matrix in cancer, Nat. Rev. Cancer 21 (2021) 217–238.
[35] T.R. Cox, J.T. Erler, Molecular pathways: connecting fibrosis and solid tumor metastasis, Clinical Cancer Research: An Official Journal of the American Association for Cancer Res. 20 (2014) 3637–3643.
[36] S.M. Abdel-Hafez, J. Zapp, M. Gallei, M. Schneider, Formulation attributes, acid tunable degradability and cellular interaction of acetalated maltodextrin nanoparticles, Carbohydr. Polym. 288 (2022) 119378.
[37] M. Marques, R. Löbenberg, M. Almukainzi, Simulated biological fluids with possible application in dissolution testing, Dissolut. Technol. 18 (2011) 15–28.
[38] A. Torge, G. Pavone, M. Jurisic, K. Lima-Engelmann, M. Schneider, A comparison of spherical and cylindrical microparticles composed of nanoparticles for pulmonary application, Aerosol Sci. Tech. 53 (2019) 53–62.

[39] N.A. Stocke, S.A. Meenach, S.M. Arnold, H.M. Mansour, J.Z. Hilt, Formulation and characterization of inhalable magnetic nanocomposite microparticles (MnMs) for targeted pulmonary delivery via spray drying, Int. J. Pharm. 479 (2015) 320–328.
[40] T. Hibbard, H. Mitchell, Y. Kim, K. Shankland, H. Al-Obaidi, Spray dried progesterone formulations for carrier free dry powder inhalation, Eur. J. Pharm. Biopharm. 189 (2023) 264–275.
[41] I. Yakavets, A. Francois, A. Benoit, J.-L. Merlin, L. Bezdetnaya, G. Vogin, Advanced co-culture 3D breast cancer model for investigation of fibrosis induced by external stimuli: optimization study, Sci. Rep. 10 (2020) 21273.
[42] S.J. Han, S. Kwon, K.S. Kim, Challenges of applying multicellular tumor spheroids in preclinical phase, Cancer Cell Int. 21 (2021) 152.
[43] C.A. Lima, P.M.B. Rodrigues, T.S. Porto, D.A. Viana, J.L. Lima Filho, A.L.F. Porto, M.G. Carneiro da Cunha, Production of a collagenase from Candida albicans URM3622, Biochem. Eng. J. 43 (2009) 315–320.
[44] D.A. Fernandes, E. Costa, P. Leandro, M.L. Corvo, Formulation of spray dried enzymes for dry powder inhalers: an integrated methodology, Int J Pharm 615 (2022) 121492.
[45] R.Y.K. Chang, M.Y.T. Chow, D. Khanal, D. Chen, H.-K. Chan, Dry powder pharmaceutical biologics for inhalation therapy, Adv. Drug Deliv. Rev. 172 (2021) 64–79.
[46] D.A. Fernandes, P. Leandro, E. Costa, M.L. Corvo, Dry powder inhaler formulation of Cu, Zn-superoxide dismutase by spray drying: a proof-of-concept, Powder Technol. 389 (2021) 131–137.
[47] S. Focaroli, P.T. Mah, J.E. Hastedt, I. Gitlin, S. Oscarson, J.V. Fahy, A.M. Healy, A design of experiment (DoE) approach to optimise spray drying process conditions for the production of trehalose/leucine formulations with application in pulmonary delivery, Int. J. Pharm. 562 (2019) 228–240.
[48] N. Alhajj, N.J. O'Reilly, H. Cathcart, Quality by design – spray drying of ciprofloxacin-quercetin fixed-dose combination intended for inhalation, Int. J. Pharm. 642 (2023) 123151.
[49] N. Alhajj, N.J. O'Reilly, H. Cathcart, Leucine as an excipient in spray dried powder for inhalation, Drug Discov. Today 26 (2021) 2384–2396.
[50] U.V. Shah, V. Karde, C. Ghoroi, J.Y.Y. Heng, Influence of particle properties on powder bulk behaviour and processability, Int. J. Pharm. 518 (2017) 138–154.
[51] R. Vehring, Pharmaceutical particle engineering via spray drying, Pharm. Res. 25 (2008) 999–1022.
[52] M.A.M. Momin, I.G. Tucker, C.S. Doyle, J.A. Denman, S. Sinha, S.C. Das, Co-spray drying of hygroscopic kanamycin with the hydrophobic drug rifampicin to improve the aerosolization of kanamycin powder for treating respiratory infections, Int. J. Pharm. 541 (2018) 26–36.
[53] Y.-X. Chang, J.-J. Yang, R.-L. Pan, Q. Chang, Y.-H. Liao, Anti-hygroscopic effect of leucine on spray-dried herbal extract powders, Powder Technol. 266 (2014) 388–395.
[54] L. Li, S. Sun, T. Parumasivam, J.A. Denman, T. Gengenbach, P. Tang, S. Mao, H.-K. Chan, l-Leucine as an excipient against moisture on in vitro aerosolization performances of highly hygroscopic spray-dried powders, Eur. J. Pharm. Biopharm. 102 (2016) 132–141.
[55] P. Zanen, L.T. Go, J.W. Lammers, The efficacy of a low-dose, monodisperse parasympathicolytic aerosol compared with a standard aerosol from a metered-dose inhaler, Eur. J. Clin. Pharmacol. 54 (1998) 27–30.
[56] J. López-García, M. Lehocký, P. Humpolíček, P. Sáha, HaCaT keratinocytes response on antimicrobial atelocollagen substrates: extent of cytotoxicity, cell viability and proliferation, J. Funct. Biomater. 5 (2014) 43–57.
[57] M. Kato, Y. Hattori, M. Kubo, Y. Maitani, Collagenase-1 injection improved tumor distribution and gene expression of cationic lipoplex, Int. J. Pharm. 423 (2012) 428–434.
[58] L. Eikenes, S. Bruland Ø, C. Brekken, L. Davies Cde, Collagenase increases the transcapillary pressure gradient and improves the uptake and distribution of monoclonal antibodies in human osteosarcoma xenografts, Cancer Res. 64 (2004) 4768–4773.
[59] R.Z. Lin, H.Y. Chang, Recent advances in three-dimensional multicellular spheroid culture for biomedical research, Biotechnol. J. 3 (2008) 1172–1184.
[60] B.M. Leung, S.C. Lesher-Perez, T. Matsuoka, C. Moraes, S. Takayama, Media additives to promote spheroid circularity and compactness in hanging drop platform, Biomater. Sci. 3 (2015) 336–344.
[61] N.A. Slawny, M. Labant, Physiologically relevant spheroid models for three-dimensional cell culture, Technology Platforms for 3D Cell Culture (2017) 50–73.
[62] N. Hari, P. Patel, J. Ross, K. Hicks, F. Vanholsbeeck, Optical coherence tomography complements confocal microscopy for investigation of multicellular tumour spheroids, Sci. Rep. 9 (2019) 10601.